Ocean Systems Engineering, *Vol. 15, No. 4 (2025) 387-406*
https://doi.org/10.12989/ose.2025.15.4.387

Imaging sonar based active viewpoint adjustment for underwater SLAM in structured environments

Geonwoo Park[1a], Dongsub Kim[2b], Bonchul Ku[2c], Seungwon Ham[2d], Sungduk Kim[3e], Jinbeom Kim[3f] and Son-Cheol Yu[*2]

[1]Division of Advanced Nuclear Engineering, Pohang University of Science and Technology (POSTECH), 77 Cheongam-ro, Nam-gu, Pohang-si, Gyeongbuk 37673, Republic of Korea
[2]Department of Convergence IT Engineering, Pohang University of Science and Technology (POSTECH), 77 Cheongam-ro, Nam-gu, Pohang-si, Gyeongbuk 37673, Republic of Korea
[3]Maritime RD Center, LIG Nex1, 333 Pangyo-ro, Bundang-gu, Seongnam-si, Gyeonggi-do 13488, Republic of Korea

(Received November 10, 2025, Revised December 2, 2025, Accepted December 6, 2025)

Abstract. Simultaneous localization and mapping (SLAM) is a critical capability for any autonomous underwater vehicle (AUV) in various underwater applications, including infrastructure inspection and seabed exploration. However, achieving robust and accurate state estimation in such environments remains a significant hurdle. This is primarily attributable to the inherent scarcity of geometric features in the subsea environment itself and the limited field of view (FoV) of imaging sonar used for feature acquisition. These factors collectively elevate the probability of iterative closest point (ICP) degeneracy, a frequent challenge in most SLAM solutions. To overcome this limitation, this study proposes a method that actively adjusts the imaging sonar's viewpoint to achieve more reliable ICP results and improve SLAM performance. First, we introduce a 2D tensor voting-based geometric descriptor to quantify the geometric information of features extracted from the sonar, enabling real-time assessment of degeneracy risk. Second, in viewpoints where degeneracy is anticipated, the sonar viewpoint is actively adjusted to acquire a more geometrically rich perspective. Third, omnidirectional features obtained during the viewpoint adjustment process are integrated as new keyframes into the SLAM graph, providing additional constraints. Our experimental validation comprises both a field feasibility test and simulations. The field feasibility test, conducted in a real underwater structured environment, confirmed the inherent scarcity of geometrically rich features in actual data acquisition. Subsequently, simulation experiments mimicking three underwater structured environments, including harbor and offshore oil rig structures, were performed. The results showed that the proposed method improved both the absolute trajectory error (ATE) and the ICP matching success rate compared to conventional fixed-sonar-heading SLAM even when following an identical trajectory in both methods.

Keywords: AUV; ICP degeneracy; scan matching; tensor voting; underwater localization

∗Corresponding author, Professor, E-mail: sncyu@postech.ac.kr
[a] M.Sc. Student, E-mail: pj012356@postech.ac.kr
[b] M.Sc. Student, E-mail: kbs7517@postech.ac.kr
[c] Integrated M.S./Ph.D. Student, E-mail: bonchulku@postech.ac.kr
[d] M.Sc. Student, E-mail: gkatmddnjs10@postech.ac.kr
[e] Researcher, E-mail: sungduk.kim@lignex1.com
[f] Researcher, E-mail: jinbeom.kim@lignex1.com

http://www.techno-press.org/?journal=ose&subpage=7 ISSN: 2093-6702 (Print), 2093-677X (Online)

1. Introduction

Underwater autonomous navigation and mapping are essential technologies in various underwater applications, including marine infrastructure inspection, underwater archaeology, environmental monitoring, and seabed resource exploration. As autonomous underwater vehicles (AUVs) and remotely operated vehicles (ROVs) increasingly operate in complex and unknown subsea environments, a robust simultaneous localization and mapping (SLAM) system is becoming crucial for safe and efficient mission execution.

Unlike terrestrial environments where optical sensors such as cameras and light detection and ranging (LiDAR) provide rich geometric information, electromagnetic waves rapidly attenuate in water because of its physical properties. This makes the use of electromagnetic sensors impossible or limits their effective range to a few meters or less (Joshi *et al.* 2019, Joshi *et al.* 2022). Consequently, sonar, an acoustic sensor, is employed as the reliable perception system for AUVs. In particular, forward-looking imaging sonar can operate effectively over distances of tens of meters, largely independent of water turbidity and lighting conditions, making it a vital sensor in underwater SLAM applications (Pyo *et al.* 2015, Stokey *et al*. 2005, Singh *et al*. 2004, Nakatani *et al.* 2008, McConnell *et al*. 2022a, McConnell *et al*. 2020).

Many SLAM systems, including underwater SLAM systems, rely on iterative closest point (ICP) scan matching to estimate the relative transformations between consecutive scans, thereby estimating the AUV's motion (McConnell *et al.* 2022b, McConnell *et al.* 2022a, McConnell *et al.* 2025). However, the ICP-based approach faces challenges in planar or featureless environments, where the lack of geometric constraints leads to ambiguous correspondence and unreliable pose estimation (Lee *et al.* 2025, Tuna *et al*. 2024, Zhang *et al.* 2016, Hinduja *et al.* 2019). In such cases, the ICP solution is untrustworthy and introduces significant drift in the graph optimization solution.

These fundamental limitations of ICP are further aggravated by the intrinsic physical constraints of imaging sonar and the nature of the marine and underwater environment. Unlike LiDAR, which is widely utilized in terrestrial SLAM systems and provides 360◦ omnidirectional coverage with consistent signal quality, underwater imaging sonar generally has a restricted horizontal field of view (FoV). Moreover, due to its relatively higher operating frequency compared to other sonars, the signal suffers severe attenuation with distance (Sun *et al*. 2021). This results in a trade-off for imaging sonar: achieving high-resolution, reliable point clouds conflicts with obtaining geometrically rich point clouds across a wide FoV. Furthermore, the marine environment frequently contains uniform and repetitive structures which makes it difficult to obtain geometrically rich features for reliable ICP registration (Guth *et al*. 2014). Additionally, controlling an AUV is inherently more challenging than controlling a ground robot due to the dominance of high hydrodynamic drag and inertial effects in underwater environments. Frequently changing the vehicle's body heading consumes more energy and can negatively affect control precision and stability (Fossen 2011). Therefore, simply adjusting the AUV's heading to acquire geometrically rich data may be inefficient in terms of energy consumption and control stability. These sensor and environmental characteristics restrict an AUV's ability to acquire geometrically rich data, which in turn increases the probability of a degenerate ICP result.

To overcome the aforementioned limitations, this paper proposes an active imaging sonar viewpoint adjustment method to improve the reliability of ICP results. Fig. 1 describes the overall concept of this proposed method, illustrating how the AUV actively seeks optimal viewpoints. Specifically, the system utilizes a 2D tensor voting-based geometric descriptor to quantify the

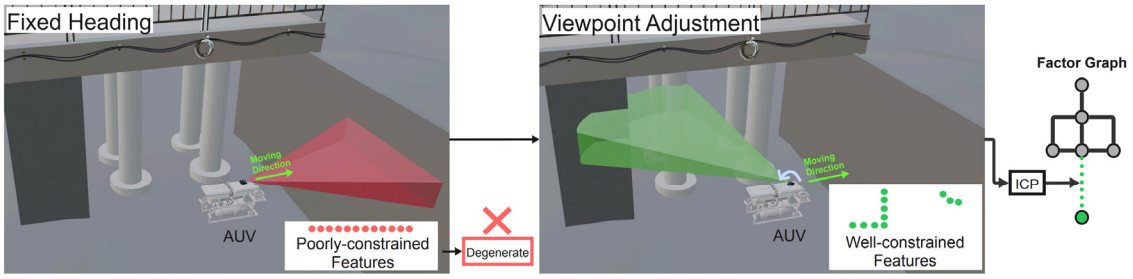

Fig. 1 Conceptual illustration of the proposed method

geometric richness and constraint strength of the acquired sonar features in real-time. If an area is detected where ICP degeneracy is anticipated due to a lack of geometric features, the system actively adjusts the sonar direction to acquire a viewpoint containing richer and more distinguishable geometric structures using the geometric descriptor. Furthermore, the omnidirectional features collected during this viewpoint adjustment process are integrated as new keyframes into the SLAM graph, providing additional constraints for overall trajectory optimization. This active sensing strategy enables the AUV to achieve more robust and accurate SLAM performance, even in feature-sparse underwater structured environments.

2. Related works

2.1 Underwater SLAM with sonar

Although various sensors, including optical cameras, have been used as external perception sensors to solve the underwater SLAM problem (Xu *et al.* 2025, Zhao *et al.* 2023, Song *et al*. 2024, Joshi *et al.* 2019), electromagnetic wave-based sensors have a limitation: they are heavily dependent on the water's turbidity, leading to rapid signal attenuation in water (Joshi *et al.* 2019). To overcome these constraints, research utilizing sonar sensors has been actively pursued, which can be broadly divided into two categories.

First, there is the approach of utilizing sonar sensors as auxiliary sensors for optical camera-based SLAM. Rahman et al. Tightly coupled sonar-visual-inertial-depth formulation **(**SVIn), which combines a scanning imaging sonar with a vision-inertial framework, demonstrating improved performance in submerged bus and underwater cave environments (Rahman *et al.* 2018, Rahman *et al*. 2019). More recently, robust underwater SLAM with sonar optimization **(**RUSSO), proposed by Pan *et al*. (2025), is a sonar-vision-inertial fusion SLAM that achieves robust trajectory estimation by supplementarily applying sonar constraints when vision-based estimation degenerates. In this capacity, sonar has primarily functioned as a complementary sensor to mitigate the instability of vision-based SLAM. However, due to the nature of optics, performance remains dependent on water turbidity and lighting, making it difficult to achieve generalized performance across diverse underwater environments.

Second, research utilizing sonar as the primary sensor has been continually proposed. Johannsson *et al*. implemented pose graph SLAM for harbor surveillance missions by integrating imaging sonar registration with doppler velocity log (DVL)/ inertial measurement unit (IMU) (Johannsson *et al.* 2010). Fallon *et al.* enabled long-term feature re-observation without external

beacons through sonar-based loop closure for repetitively observed structures (Fallon *et al.* 2013). Westman et al. proposed a method to incorporate landmarks extracted from imaging sonar into graph optimization, distinguishing between cases with sufficient and insufficient constraint information (Westman *et al.* 2018). McConnell and Englot addressed the drift issue in sonar-based SLAM by integrating external surface imagery into the factor graph (McConnell *et al*. 2022a) and presented a 3D predictive technique for repetitive structures (McConnell *et al.* 2021). To address the loss of elevation information in sonar, a method of orthogonally arranging multiple sonars was also proposed (McConnell *et al.* 2020). However, despite these efforts, most imaging sonar-based SLAM approaches still cannot fully compensate for the lack of elevation information. Consequently, they typically project the acquired data onto a two-dimensional plane, which further limits the diversity of observable features. This dimensional reduction exacerbates the possibility of ICP degeneracy, as the available geometric constraints become even more restricted.

2.2 Degeneracy in ICP and mitigation strategies

As mentioned earlier, the ICP algorithm is a core method for registering sensor data in SLAM systems, but it can encounter the ICP degeneracy problem in planar or feature-sparse environments. This degradation compromises the accuracy and robustness of trajectory estimation, leading to various proposed solutions. These studies are predominantly LiDAR-based and can be classified into three major categories.

The first approach is based on analyzing the hessian matrix eigenvalues of the ICP cost function. These methods identify cases where the geometric constraint is weak in a specific direction based on the magnitude of the eigenvalues (Zhang *et al*. 2016, Hinduja *et al*. 2019, Nashed *et al.* 2021). However, this method is fundamentally limited by its heavy reliance on setting empirical thresholds for the eigenvalues, making generalization across diverse environments or sensor configurations difficult.

The second approach involves quantitative metrics and probabilistic ICP variants. To overcome the limitations of empirical thresholds, more generalized and robust approaches have been proposed. X-ICP (Tuna *et al*. 2024) introduced a localizability metric to quantitatively assess the degree of geometric constraint of ICP registration and restricted updates in poorly constrained directions, enabling robust registration even in extreme environments. Furthermore, Hatleskog and Alexis proposed the probability of degeneracy for each direction based on the noise characteristics of points and normals, offering a probabilistic ICP variant that gently attenuates updates (Hatleskog and Alexis 2024). These methods go beyond the limitations of threshold-based approaches, enabling more robust degeneracy mitigation that accounts for the variety of environments and sensors. However, these approaches also assume the use of sensors like LiDAR, which provide a wide FoV (360◦ or broad field of view) and relatively abundant features in real time, thereby limiting their effectiveness in resolving the fundamental problem of feature scarcity encountered when using imaging sonar in underwater environments.

The third approach involves learning-based degeneracy prediction methods. These attempts aim to predict degeneracy directly from data (Nobili *et al.* 2018, Nubert *et al*. 2022). While they possess the potential to achieve generalized performance based on data, they suffer from drawbacks such as the high cost of generating high-quality labeled data and high computational complexity due to intricate models, restricting their real-time application.

In conclusion, existing research on underwater SLAM with sonar, whether utilizing sonar as an auxiliary sensor or as the primary modality, faces fundamental limitations. Approaches that

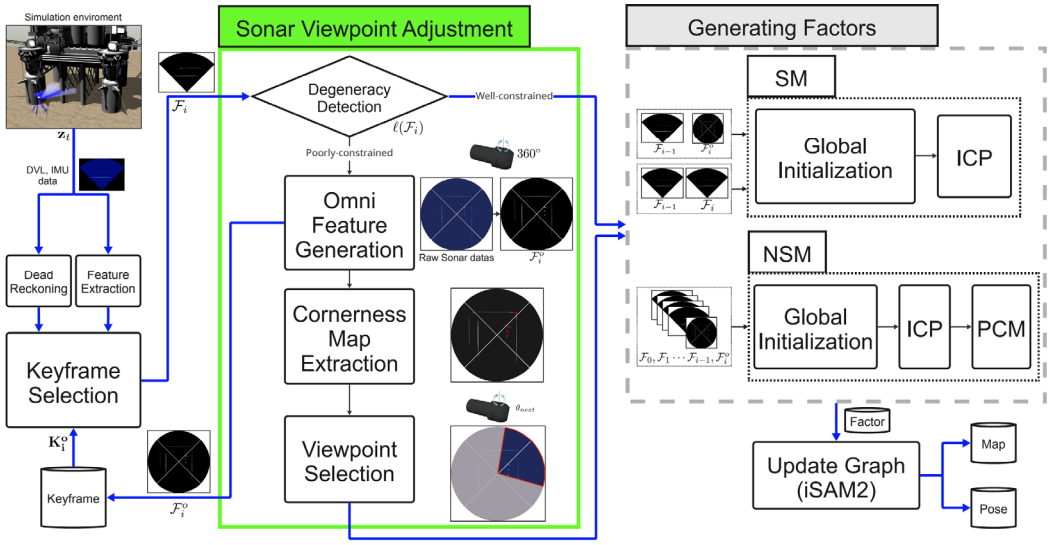

Fig. 2 System architecture of the proposed method. Acronyms: doppler velocity log(DVL), inertial measurement unit (IMU), iterative closest point (ICP), sequential matching (SM), non-sequential matching (NSM), pairwise consistent measurement (PCM), and incremental smoothing and mapping (iSAM2)

integrate vision are constrained by water turbidity and lighting, while dedicated sonar-based SLAM, particularly those using imaging sonar, suffer from a restricted FoV and the necessity of 2D projection, which further exacerbates the lack of geometric constraint. Concurrently, most state-of-the-art ICP degeneracy mitigation studies have been developed for sensors like LiDAR, which inherently provide a wide FoV and rich environmental features. In contrast, underwater imaging sonar is highly susceptible to the degeneracy issue because of its unique constraints, including a narrow FoV and the feature scarcity of the underwater environment. Therefore, reliance solely on existing ICP degeneracy mitigation methods is insufficient for SLAM performance improvement in underwater structured environments. A new approach focused on securing geometric richness in the sensor data itself is essential. To overcome these limitations, this study introduces a tensor voting-based geometric descriptor and an active viewpoint adjustment module to dynamically secure a set of features favorable for ICP registration, thereby achieving highly reliable ICP results and enhancing SLAM localization performance.

3. Proposed method

In Fig. 2, the overall process of the proposed method is described. As described in Fig. 2, it extends the conventional SLAM framework by incorporating a sonar viewpoint adjustment module. On the left side of Fig. 2, real-time data acquisition is performed using an imaging sonar, from which features are extracted. Meanwhile, odometry is estimated through dead reckoning by integrating data from the DVL and IMU sensors. When sufficient movement is detected based on the estimated odometry, the current frame is designated as a keyframe. Before performing ICP between keyframes, the sonar viewpoint adjustment module is activated. If the geometric information of the extracted features is insufficient—indicating potential ICP degeneracy—the

AUV performs omnidirectional observations to acquire additional features. Subsequently, it selects an optimal observation angle based on a cornerness metric using geometric descriptor of features and adjusts the sonar viewpoint accordingly. On the right side of Fig. 2, a factor-graph-based SLAM framework is employed to integrate the keyframes and factors, followed by optimization using iSAM2. Through this pipeline, the AUV can evaluate degeneracy risk in real time and actively modify its viewpoint to achieve more stable and accurate registration. The following sections describe each component of the pipeline in greater detail, focusing primarily on the sonar viewpoint adjustment process.

3.1 Problem description

We define the SLAM problem as the estimation of both the three-dimensional pose of the AUV and the corresponding two-dimensional map. Let t denote a discrete timestep, and the AUV pose at time t be represented as $\mathbf{x}_t$

$$\mathbf{x}_t = (x, y, \theta)^{\mathsf{T}} \tag{1}$$

Each $\mathbf{x}_t$ is associated with a set of sonar observations $\mathbf{z}_t$. The observation set $\mathbf{z}_t$ consists of sonar signals characterized by range $R \in R+$, bearing $\theta \subseteq [-\pi,\pi)$, elevation $\phi \subseteq [-\pi,\pi)$, and intensity value $\gamma \in R+$. The conversion of these sonar measurements from polar to Cartesian coordinates is given by

$$\begin{pmatrix} X \\ Y \\ Z \end{pmatrix} = R \begin{pmatrix} \cos\phi \cos\theta \\ \cos\phi \sin\theta \\ \sin\phi \end{pmatrix} \tag{2}$$

where (X,Y,Z) represents the Cartesian coordinates of each measurement. Each observation $\mathbf{z}_t$ also includes the AUV's linear velocity $\in R$ and rotational velocity $\in R$ at time t. Assuming a constant depth operation, the AUV motion follows the following dynamics model

$$\mathbf{x}_t = \mathbf{g}(\mathbf{u}_t, \mathbf{x}_{t-1}) + \boldsymbol{\delta}_t, \tag{3}$$

where $\mathbf{u}_t$ denotes the control command and $\boldsymbol{\delta}_t$ represents the process noise. The objective of SLAM is to jointly estimate the entire trajectory $\mathbf{x}_{1:t}$ and the map $\mathbf{m}$, which can be expressed as the following posterior distribution

$$p(\mathbf{x}_{1:t}, \mathbf{m} \mid \mathbf{u}_{1:t}, \mathbf{z}_{1:t}) \quad . \tag{4}$$

3.2 Graph-based SLAM

To estimate both the position of the AUV and the surrounding map, this study adopts a graph based SLAM paradigm (Grisetti *et al*. 2010, Cadena *et al*. 2016). The graph-based SLAM framework consists of two main components: the front-end and the back-end. The front-end is responsible for sensor signal preprocessing, feature extraction, and feature-based relative pose estimation, while the back-end estimates the overall trajectory and map through factor graph optimization. The complete trajectory of the AUV is defined as

$$\mathbf{X} = \{\mathbf{x}_0, \mathbf{x}_1, \ldots, \mathbf{x}_N\} \tag{5}$$

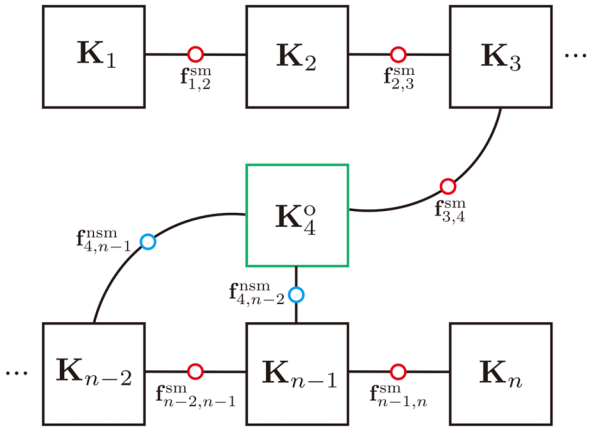

Fig. 3 Example of the factor graph for the proposed method

where $\mathbf{x}_i \in \mathrm{SE}(2)$ represents the AUV pose at the i-th timestep. Each pose $\mathbf{x}_i$ consists of rotation and translation components

$$\mathbf{x}_i = \begin{bmatrix} \mathbf{R}(\theta_i) & \mathbf{t}_i \\ 0 & 1 \end{bmatrix}, \ \mathbf{t}_i = \begin{bmatrix} x_i \\ y_i \end{bmatrix} \tag{6}$$

Each pose $\mathbf{x}_i$ forms a keyframe $\mathbf{K}_i$ along with the set of extracted features F_i. Since sonar data typically have a low signal-to-noise ratio (SNR), the constant false alarm rate (CFAR) algorithm, commonly used in low-SNR radar and sonar applications (El-Darymli *et al*. 2013, Acosta and Villar 2014, Wang *et al*. 2022), was adopted for feature extraction. Among several CFAR variants, the smallest-of-cell-averaging (SOCA) method was specifically utilized. The points extracted via CFAR are converted to cartesian coordinates according to Eq. (2). Since elevation angle ϕ cannot be obtained directly from sonar data, it is set to zero during conversion. The relative pose constraint between two keyframes $\mathbf{K}_i$ and $\mathbf{K}_j$ is expressed as a factor $\mathbf{f}_i$

$$\mathbf{f}_{ij} : (\mathbf{x}_i, \mathbf{x}_j) \ \longmapsto \ \Delta\mathbf{x}_{ij} \in SE(2) \tag{7}$$

As shown in Fig. 3, two types of factors, $\mathbf{f}^{s}_{ij}$ and $\mathbf{f}^{ns}_{ij}$, are defined to represent the relations between the two types of keyframes, $\mathbf{K}_i$ and $\mathbf{K}^{o}_i$. Sequential factors $\mathbf{f}^{s}_{ij}$ represent relative pose constraints between consecutive keyframes, while non-sequential factors $\mathbf{f}^{ns}_{ij}$ (loop-closing factors) represent constraints between non-adjacent keyframes. The standard keyframe $\mathbf{K}_i$ contains features $\mathcal{F}_i$ acquired at a single viewpoint, whereas $\mathbf{K}^{o}_i$ includes omnidirectional features obtained through 360◦ sonar rotation. Each factor $\mathbf{f}_{ij}$ is derived from the ICP-based scan matching between $\mathcal{F}_i$ and $\mathcal{F}_j$, yielding a relative transformation $\Delta\mathbf{x}_{ij}$ along with an associated covariance matrix $\mathbf{\Sigma}_{ij}$ that represents estimation uncertainty

$$\mathbf{\Sigma}_{ij} = \mathrm{diag}(\sigma_x^2, \ \sigma_y^2, \ \sigma_\theta^2). \tag{8}$$

Because feature correspondences between $\mathcal{F}_i$ and $\mathcal{F}_j$ are initially unknown, the ICP solution can easily become trapped in local minima. To mitigate this issue, an initial transformation is provided to ICP using dead-reckoning estimates and consensus sets, following the approach of (Fischler and Bolles 1981). For each factor $\mathbf{f}_{ij}$, an error term $\mathbf{e}_{ij}$ is defined, and the overall cost function can be

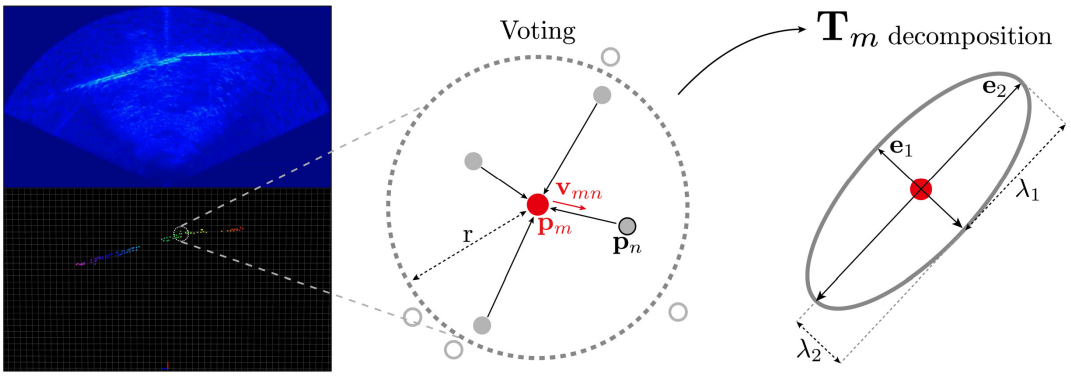

Fig. 4 Illustration of 2D tensor voting from the extracted imaging sonar features

formulated using the corresponding covariance $\mathbf{\Sigma}_{ij}$. The optimization seeks the optimal trajectory X^* that minimizes the total weighted error

$$\mathbf{X}^* = \underset{\mathbf{X}}{\operatorname{argmin}} \sum_{(i,j)} \mathbf{e}_{ij}^{\top} \mathbf{\Sigma}_{ij} \mathbf{e}_{ij}. \tag{9}$$

3.3 Geometric descriptor via 2D tensor voting

To detect features that may lead to ICP degeneracy and to identify those that can ensure reliable ICP results within the proposed method, it is crucial to have a descriptor capable of quantitatively representing the geometric information of acquired features. For this purpose, we employ the tensor voting method based on a second-order structure tensor, which quantitatively characterizes the geometric properties of $\mathcal{F}$ (Wu *et al*. 2012). We define the tensor $\mathbf{T}_m$ to encode the geometric information of each feature point $\mathbf{p}_m$. $\mathbf{T}_m$ represents the local geometric structure of $\mathbf{p}_m$ by aggregating the directional distributions of neighboring points with weights. The computation of $\mathbf{T}_m$ proceeds as follows and illustrated in Fig. 4. For a reference point $\mathbf{p}_m = [x_m, y_m]^{\top}$, a neighborhood set $\mathbf{p}_m \in \mathcal{N}(m)$ is selected within a radius r. The distance and unit direction vector between $\mathbf{p}_m$ and each neighboring point $\mathbf{p}_n$ are defined as

$$d_{mn} = \|\mathbf{p}_n - \mathbf{p}_m\|_2, \tag{10}$$

$$\mathbf{v}_{mn} = \frac{\mathbf{p}_n - \mathbf{p}_m}{\|\mathbf{p}_n - \mathbf{p}_m\|_2} = \begin{bmatrix} v_x \\ v_y \end{bmatrix} \tag{11}$$

and the corresponding weight is defined as

$$w_{mn} = e^{\left(-\frac{d_{mn}^2}{2\sigma^2}\right)} \tag{12}$$

where σ_i is an adaptive scale determined by the mean distance of the k nearest neighbors among $\{\mathbf{p}_1, \mathbf{p}_2, \ldots, \mathbf{p}_M\}$ that compose $\mathcal{F}$. Each neighboring point $\mathbf{p}_n$ votes to the reference point $\mathbf{p}_m$ with a second-order moment of the form

$$\mathbf{v}_{mn}\mathbf{v}_{mn}^{\top} = \begin{bmatrix} v_x^2 & v_x v_y \\ v_x v_y & v_y^2 \end{bmatrix} \tag{13}$$

and the tensor is defined as the weighted sum of these moments

$$\mathbf{T}_m = \sum_{n\in\mathcal{N}(m)} w_{mn}\,\mathbf{v}_{mn}\mathbf{v}_{mn}^{\top} \tag{14}$$

$$= \begin{bmatrix} \sum_n w_{mn} v_x^2 & \sum_n w_{mn} v_x v_y \\ \sum_n w_{mn} v_x v_y & \sum_n w_{mn} v_y^2 \end{bmatrix} \tag{15}$$

$\mathbf{T}_m$ is a second-order symmetric tensor that encapsulates the local geometric properties of $\mathbf{p}_m$ within $\mathcal{F}$, implying both the principal direction and the degree of isotropy or anisotropy determined by its local neighborhood structure. Performing eigenvalue decomposition on $\mathbf{T}_m$ yields the eigenvalues λ_1, λ_2 and the corresponding eigenvectors $\mathbf{e}_1$ and $\mathbf{e}_2$ as follows

$$\mathbf{T}_m = \mathbf{U}_m\mathbf{\Lambda}_m\mathbf{U}_m^{\top} = [\mathbf{e}_1\mathbf{e}_2]\begin{bmatrix}\lambda_1 & 0\\ 0 & \lambda_2\end{bmatrix}\begin{bmatrix}\mathbf{e}_1^{\top}\\ \mathbf{e}_2^{\top}\end{bmatrix} \tag{16}$$

Using this formulation, a set of tensors $\{\mathbf{T}_1, \mathbf{T}_2, \ldots, \mathbf{T}_M\}$ containing the geometric information of all points in $\mathcal{F}$ can be obtained. Those are later utilized for detecting potential ICP degeneracy and for sonar viewpoint selection.

3.4 Sonar viewpoint adjustment using omnidirectional features

When the AUV determines that ICP degeneracy is likely to occur in planar or feature-sparse scenes, it actively adjusts the sonar viewpoint to acquire richer geometric information. This process consists of three stages: degeneracy detection, omnidirectional feature acquisition through 360° rotation, and viewpoint selection based on cornerness.

3.4.1 Degeneracy detection

When the AUV determines that the currently acquired $\mathcal{F}_i$ may cause ICP degeneracy, it is preferable not to generate an ICP-based factor for that keyframe so that the corresponding outlier is not reflected in graph optimization. To evaluate whether the acquired $\mathcal{F}_i$ is well-constrained in the state space, we define the spatial constraint metric $\ell(\mathcal{F}_i)$ using the geometric information tensors $\mathbf{T}_1,\ldots,\mathbf{T}_M$ computed for each feature in $\mathcal{F}_i$. The principal eigenvector $\mathbf{e}_1^m$ of each tensor $\mathbf{T}_m$ represents the dominant local direction of the corresponding point. If $\mathcal{F}_i$ forms a feature set that provides sufficient constraints in the estimated state space, the eigenvectors $\mathbf{e}_1,\ldots,\mathbf{e}_m$ are expected to exhibit diverse orientations. Conversely, if the eigenvectors are predominantly aligned in a similar direction, the constraints imposed by $\mathcal{F}_i$ are limited, indicating that the ICP result is likely to degenerate. The spatial constraint metric $\ell(\mathcal{F}_i)$ is defined as follows. Let each principal eigenvector be normalized as

$$\mathbf{u}_k = \frac{\mathbf{e}_1^{(k)}}{\left\|\mathbf{e}_1^{(k)}\right\|_2}, k = 1, \ldots, n, \tag{17}$$

then $\ell(\mathcal{F}_i)$ can be expressed as

$$\ell(\mathcal{F}_i) = \left\|\frac{1}{n}\sum_{k=1}^{n}\mathbf{u}_k\right\|_2 \tag{18}$$

By applying the triangle inequality, it follows that

$$\left\| \frac{1}{n} \sum_{k=1}^{n} \mathbf{u}_k \right\|_2 \leq \frac{1}{n} \sum_{k=1}^{n} \|\mathbf{u}_k\|_2 = \frac{1}{n} \cdot n = 1 \tag{19}$$

and since the euclidean norm is non-negative, the lower bound is 0. Therefore, the following condition holds

$$0 \leq \ell(\mathrm{F}_i) \leq 1 \tag{20}$$

If $\ell(\mathcal{F}_i) = 1$, all directions are perfectly aligned, indicating a high likelihood of degeneracy. Conversely, if $\ell(\mathcal{F}_i) \approx 0$, $\mathcal{F}_i$ provides diverse directional constraints, implying a low probability of degeneracy. Based on this metric, the AUV can quantitatively evaluate the degeneracy likelihood of ICP in real time. When $\ell(\mathcal{F}_i)$ does not exceed a predefined threshold, an ICP factor is generated for $\mathbf{K}_i$. However, if $\ell(\mathcal{F}_i)$ exceeds the threshold, indicating a high probability of degeneracy, the AUV refrains from registering $\mathcal{F}_i$ as a keyframe and stops its motion to proceed to the omnidirectional feature acquisition stage for obtaining features more favorable to ICP.

3.4.2 Omnidirectional feature acquisition

After the previous stage, it halts its movement and performs a 360° only sonar viewpoint rotation scan to dynamically adjust the sonar viewpoint and collect features more reliable for ICP registration. Depending on the FoV of imaging sonar, a predefined set of N rotation angles $\Theta = \{\theta_1, \theta_2, \ldots, \theta_N\}$ is determined to ensure full 360° feature coverage. The imaging sonar is sequentially rotated according to Θ, acquiring a sonar image I_i at each heading θ_i, from which a set of feature points $\mathcal{F}_i = \{p_1^i, p_2^i, \ldots, p_M^i\}$ is extracted. During this process, the AUV maintains a stationary position using PID control. Each directional feature set $\mathcal{F}_i$ is transformed into the AUV's base coordinate frame through rotation. The rotation matrix $\mathbf{R}(\theta_i)$ for transforming the i-th scan is defined

$$\mathbf{R}(\theta_i) = \begin{bmatrix} \cos\theta_i & -\sin\theta_i \\ \sin\theta_i & \cos\theta_i \end{bmatrix} \tag{21}$$

and the overall omnidirectional feature set $\mathcal{F}^o$ is defined as

$$\mathcal{F}^o = \bigcup_{i=1}^{N} \mathbf{R}(\theta_i)\, \mathcal{F}_i, \tag{22}$$

The obtained $\mathcal{F}^o$ serves two purposes in the proposed method. First, as illustrated in Fig. 3, it is used to construct the keyframe $\mathbf{K}^o$ that incorporates omnidirectional features. Second, it is used to determine the next sonar viewpoint that can acquire features more reliable for ICP registration.

3.4.3 Cornerness-based viewpoint selection

To obtain reliable ICP registration within the limited FoV of an imaging sonar, it is crucial to adjust the sonar viewpoint such that the next observation includes geometrically rich features based on the previously acquired $\mathcal{F}^o$. Here, geometrically rich features refer to those that sufficiently constrain the state space. To achieve this, it is necessary to evaluate how well each feature constrains the pose state space. Existing studies (Zhang *et al.* 2016, Hatleskog and Alexis 2024, Hinduja *et al*. 2019) have assessed localizability by linearizing the error term $\mathbf{e}_i(x)$ of each correspondence in ICP and computing the jacobian $\mathbf{J}_i$, from which the hessian matrix is obtained as

$$\mathbf{H} = \sum_i \mathbf{J}_i^\top \mathbf{J}_i. \tag{23}$$

By performing eigenvalue decomposition on $\mathbf{H}$, the eigenvalues $\lambda_{1,\ldots,n}$ are used to evaluate the degree of constraint (localizability) along each degree of freedom in the state space. A smaller eigenvalue corresponding to a specific degree of freedom indicates weaker constraint in that direction, implying a higher probability of ICP degeneracy. However, in this study, our objective is to determine, prior to performing ICP, which viewpoint is most likely to include geometrically favorable features for reliable registration. Directly applying existing methods to all discrete subspaces of $\mathcal{F}^o$ while considering the sonar FoV would require performing ICP across multiple candidate viewpoints, resulting in excessive computational complexity. Therefore, without executing ICP, we define a cornerness descriptor to identify features advantageous for ICP registration. Using the tensor voting technique, a local structure tensor $\mathbf{T}$ is computed around each feature, and its eigenvalues (λ_1,λ_2) are used to quantify how well the feature constrains the state space. Features that provide balanced and sufficiently strong constraints along both principal directions correspond to corner-like structures, and their cornerness values are computed following the harris corner detector (Harris and Stephens 1988) formulation

$$c_i = \lambda_{1,i}\lambda_{2,i} - k(\lambda_{1,i}+\lambda_{2,i})^2 \tag{24}$$

where $k \in [0.04, 0.06]$ is an empirical constant controlling the trade-off between sensitivity and robustness. A smaller k increases the sensitivity of corner detection, whereas a larger k enhances robustness to noise. Features with higher cornerness values contribute to increasing the principal eigenvalues of $\mathbf{J}_i^{\mathrm{T}}\mathbf{J}_i$ in all major directions of the ICP cost function, thereby improving the conditioning of $\mathbf{H}$ and reducing the probability of degeneracy. For this reason, we compute the cornerness set $\{c_1,c_2,\ldots,c_M\}$ for all features $\{\mathbf{p}_1,\mathbf{p}_2,\ldots,\mathbf{p}_M\}$ in $\mathcal{F}^o$, filter out the top percentile of high-cornerness points, and perform density-based spatial clustering of applications with noise (DBSCAN). Among the resulting clusters, the cluster containing the largest number of points is denoted as $\mathbf{c}_{\max}$, and its centroid is represented as $\boldsymbol{c}_{\max}$. The optimal sonar viewpoint for the next scan is then computed as

$$\theta_{\text{next}} = \arctan2(\boldsymbol{c}_{max,y}, \boldsymbol{c}_{max,x}) \tag{25}$$

and the sonar viewpoint is adjusted to θ_{next}. Subsequently, ICP is performed based on the updated heading θ_{next}, and the procedure can be summarized as

$$\mathcal{S} = \left\{ \left(\mathbf{p}_k^{(i)}, \mathbf{p}_k^{(j)} \right) \middle| \, \mathbf{p}_k^{(i)} \in \mathcal{F}_i, \mathbf{p}_k^{(j)} \in \mathcal{F}_j \right\} \tag{26}$$

$$\mathbf{e}_k(\mathbf{x}) = \mathbf{R}\mathbf{R}'(\theta_{\text{next}})\mathbf{p}_k^{(i)} + \mathbf{t} - \mathbf{p}_k^{(j)} \tag{27}$$

$$\mathbf{X}^* = \underset{\mathbf{R},\mathbf{t}}{\operatorname{argmin}} \sum_{k\in\mathcal{S}} \|e_k(\mathbf{x})\|^2 \tag{28}$$

The proposed method thus allows the AUV to continuously evaluate ICP degeneracy in real time, actively acquire omnidirectional features when needed, and adjust the sonar viewpoint based on cornerness descriptor. Through this process, the system effectively secures sufficient geometric information even in feature-sparse underwater environments. This leads to improved reliability of ICP registration and overall SLAM accuracy.

4. Experiments

To establish the practical relevance of the proposed method and confirm the core challenge of feature scarcity in real-world underwater environments, a preliminary field feasibility test was

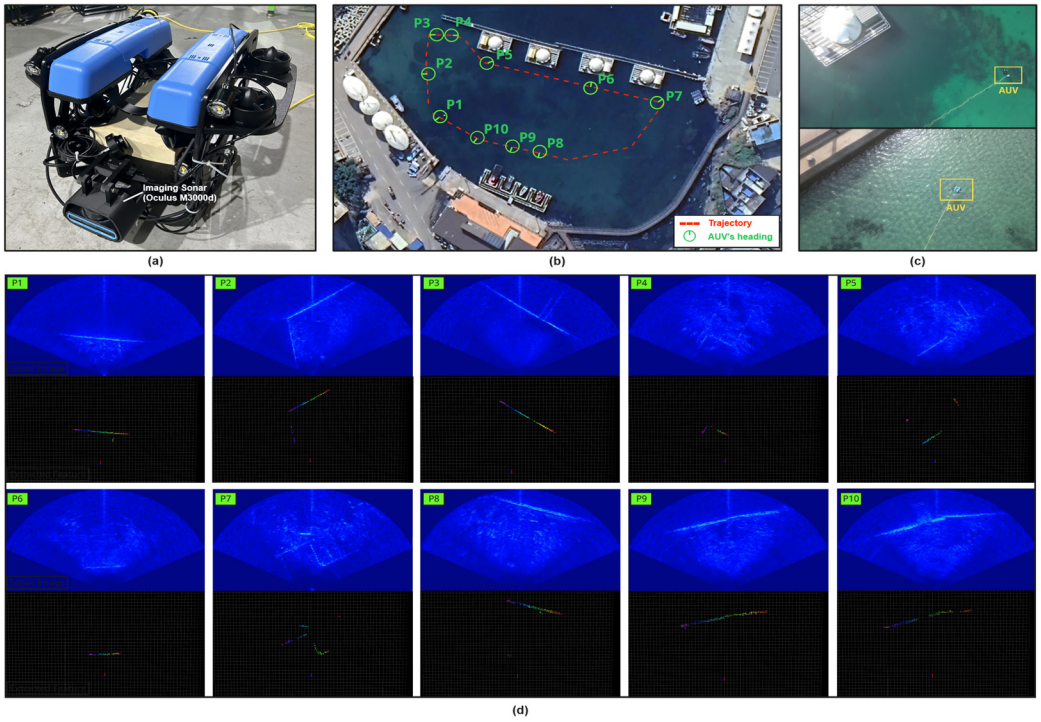

Fig. 5 Feasibility test setup and representative sonar data. (a) AUV platform: BlueROV2 equipped with an Oculus M3000d imaging sonar. (b) AUV trajectory (red dashed line) and ten indexed locations (P1–P10). (c) Test site overview at Jangil-ri fishing park. (d) Representative sonar images and SOCA-CFAR-extracted feature points obtained at sample locations shown in (b)

conducted prior to the simulation experiments. The entirety of this feasibility test, including the experimental setup, AUV trajectory, and detailed feature extraction results, is illustrated in Fig. 5.

4.1 Field feasibility test setup and purpose

The feasibility test was conducted at the Jangil-ri fishing park in Pohang, South Korea, an environment characterized by repetitive and feature-sparse underwater infrastructure. The test utilized a BlueROV2 equipped with an oculus M3000d imaging sonar for data acquisition. The primary goal of this test was to quantitatively confirm the inherent difficulty of acquiring geometrically rich features from imaging sonar data in a structured underwater environment. The AUV followed a trajectory within the experimental area, and at ten specific, indexed locations (labeled ’a’ through ’j’), sonar scans were recorded for detailed analysis.

4.2 Results: Confirmation of feature scarcity and degeneracy risk

The raw sonar scans were processed, and feature points were extracted using the SOCA-CFAR algorithm. The results clearly confirmed the initial hypothesis: the majority of the extracted features were predominantly planar or linear, indicating a high susceptibility to ICP degeneracy. Specifically, subfigures P1, P3, P6, P8, P9, and P10 in Fig. 5(d) illustrate scenarios where features

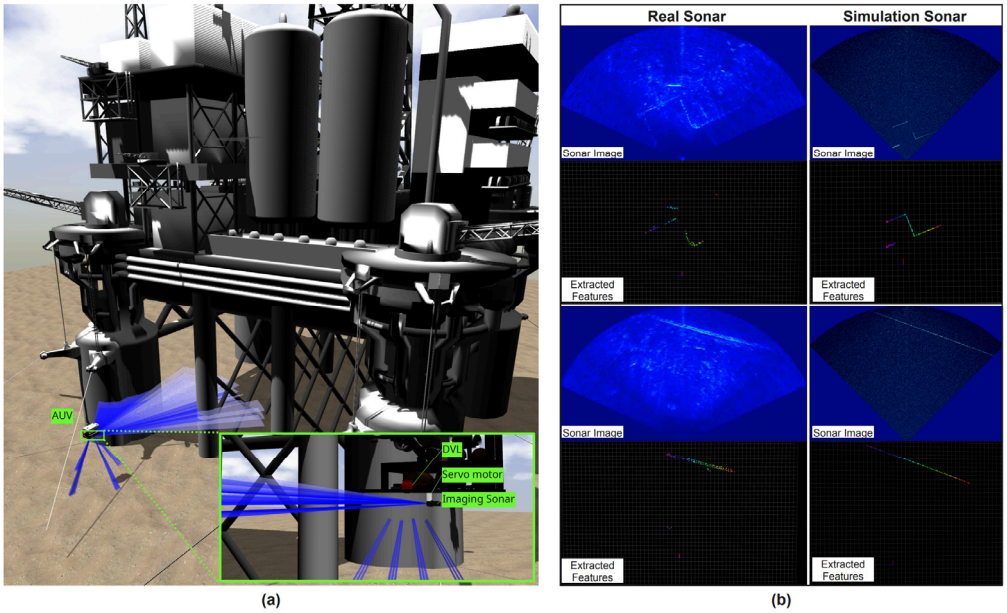

Fig. 6 Simulation overview and Sonar image comparison. (a) AUV platform and simulation setup. (b) Comparison of sonar data and feature extraction result between real-world and simulation

are linear, lacking the diverse geometric constraints necessary for reliable ICP registration, conditions that would likely lead to unreliable pose estimation and significant drift in a conventional fixed-heading SLAM system. Conversely, only a limited number of instances, such as sub-figures P2, P4, P5, and P7 in Fig. 5(d), presented features with well-constrained geometric information, which are favorable for reliable ICP registration. This field test served as a crucial validation point, demonstrating that fixed-heading imaging sonar systems are inherently constrained in real underwater structured environments due to feature sparsity, which mandates the need for an active sensing strategy to secure geometrically richer data. The subsequent simulation experiments were designed to evaluate the performance of the proposed active viewpoint adjustment method in mitigating this confirmed real-world challenge.

5. Simulation

To validate the performance of the proposed method, a series of experiments were conducted in various simulated underwater environments. This section provides a detailed explanation of the constructed simulation environments and the performance evaluation methodology.

5.1 Simulation environment setup

The simulation experiments were conducted in the robot operating system (ROS) 1 environment using the gazebo-based UUV-Simulator (Manhães *et al*. 2016), integrated with the DAVE simulator (Zhang *et al*. 2022) to simulate the imaging sonar and DVL sensors. The AUV

Fig. 7 Simulation environments used for evaluation. (a) A harbor-like structure modeled after the Jangil-ri Complex Fishing Park in Pohang, South Korea. (b) A scaled-down representation of Gamman Pier in Busan, South Korea. (c) An offshore oil rig environment simulating large-scale industrial underwater structures. Insets show real-world references for each simulated site.The inset images in (a) and (b) are screenshots from Google Maps. The inset image in (c) is publicly available [Source: https://www.nesfircroft.com/resources/blog/the-10biggest-oil-rigs-in-the-world

platform used in the experiments was based on the RexROV2 model provided by the UUV-Simulator. As illustrated in Fig. 6, a DVL and an IMU were mounted at the center of the AUV, and a rotational joint was attached to the lower center of the vehicle to function as a servo motor for controlling the viewpoint of the imaging sonar. Both the DVL and IMU sensors were configured to include gaussian noise. The imaging sonar was simulated using the BlueView m900 model implemented in the DAVE simulator, with the field of view configured to achieve real-time processing at 8 Hz on an RTX 4070 GPU. The sonar parameters were set as follows: a horizontal FoV of 90◦, a vertical FoV of 6◦, and a maximum detection range of 30 m. To enhance the realism of the simulated sonar data, various noise sources and acoustic effects observed in real underwater environments were incorporated, including speckle noise, water backscatter, impulse noise, and reverberation artifacts. Finally, the AUV's position and attitude were controlled using a PID controller, while the rotational joint for sonar viewpoint adjustment was managed by a separate PID controller.

5.2 Test scenario setup

As illustrated in Fig. 7, the experiments were conducted in three different underwater structured environments, each presenting unique geometric characteristics and challenges.

Fig. 7(a) represents a harbor environment modeled after the Jangil-ri Fishing Park in Pohang, South Korea, where only the pier structures were modeled based on satellite imagery. This environment reproduces a typical small-scale underwater infrastructure inspection scenario (60 m × 100 m). Fig. 7(b) depicts a large-scale harbor environment (150 m × 225 m) modeled after Gamman Pier in Busan, Korea, designed to produce situations where the AUV often encounters geometrically sparse data compared to the smaller harbor scenario. Fig. 7(c) represents an offshore oil rig environment (60 m × 80 m) with large cylindrical structures, designed to emulate repetitive geometric patterns and feature-scarce conditions.

In all three environments, the AUV was commanded to follow predefined waypoints at a constant velocity of 1 m/s. These waypoints were placed sufficiently close to walls or structures to ensure that the reflected signals from the imaging sonar were adequately captured, even when the

Table 1 RMSE Metric Table

	Scenario	Jangil-ri fishing park			Gamman pier			Oil rig		
	ICP error metric	Point 2 Point	Point 2 Plane	GICP	Point 2 Point	Point 2 Plane	GICP	Point 2 Point	Point 2 Plane	GICP
Fixed heading	Generated Factors (sm, nsm)	28 / 2	28 / 0	33 / 3	76 / 6	81 / 4	78 / 0	55 / 0	53 / 2	55 / 2
	Converge ratio (sm, nsm)	0.82 / 1.0	0.89 / -	0.84 / 1.0	0.81 / 1.0	0.79 / 1.0	0.86 / -	0.98 / -	0.89 / 1.0	0.91 / 1.0
	Trajectory RMSE [m]	4.317	6.316	3.997	34.94	39.80	7.93	4.56	6.76	6.15
Proposed method	Generated Factors (sm, nsm)	43 / 28	45 / 37	46 / 24	123 / 12	101 / 17	125 / 10	127 / 0	65 / 48	118 / 7
	Converge ratio (sm, nsm)	0.86 / 1.0	0.93 / 1.0	0.91 / 1.0	0.94 / 1.0	0.94 / 1.0	1.0 / 1.0	0.97 / -	0.95 / 1.0	0.96 / 1.0
	Trajectory RMSE [m]	1.029	1.657	1.515	8.9	7.1	6.60	2.38	1.27	3.65

sonar viewpoint was fixed forward. When the AUV detected feature sets with insufficient geometric constraints, it stopped to acquire omnidirectional features. The AUV's stop condition was determined by monitoring angular velocity $\mathbf{v}_{angular}$ and linear velocity $\mathbf{v}_{linear}$ obtained from the IMU and DVL sensors. The AUV was considered stationary when the most recent ten measurements simultaneously satisfied the conditions $\mathbf{v}_{angular} < \tau_{angular}$ and $\mathbf{v}_{linear} < \tau_{linear}$, where $\tau_{angular}$ and τ_{linear} are predefined small thresholds close to zero.

5.3 Comparison algorithms

The baseline SLAM framework was implemented based on codes provided in prior imaging sonar-based SLAM systems for near-shore environments (Wang *et al*. 2022, McConnell *et al.* 2022a). The overall SLAM architecture follows the structure described in Fig. 2. Since ICP performance is sensitive to both environmental conditions and the selected error metric, three representative ICP error metrics were tested under identical conditions: Point-to-Point (Besl and McKay 1992), Point-to-Plane (Chen and Medioni 1991), and Generalized ICP (Segal *et al*. 2009).

Experiments were conducted under all combinations of three environments, three ICP error metrics, and two sonar viewpoint strategies (fixed vs. proposed method), resulting in a total of 18 trials. This comprehensive design aimed to demonstrate that the proposed method consistently achieves superior estimation performance compared to fixed-heading SLAM, regardless of the ICP variant or environmental conditions. All other parameters and conditions remained identical across trials, with the only difference being the use or absence of the proposed method.

5.4 Evaluation metrics

The performance of the SLAM system was evaluated using the following quantitative metrics. The absolute trajectory error (ATE) between the estimated trajectory and the ground-truth trajectory was calculated, followed by computation of the root mean square error (RMSE) based on ATE. The ground-truth trajectory was obtained directly from the absolute position data provided by the simulation environment.

Additionally, to analyze the effect of the proposed method on ICP-based factor generation, the convergence success rates of sequential matching (SM) and non-sequential matching (NSM),

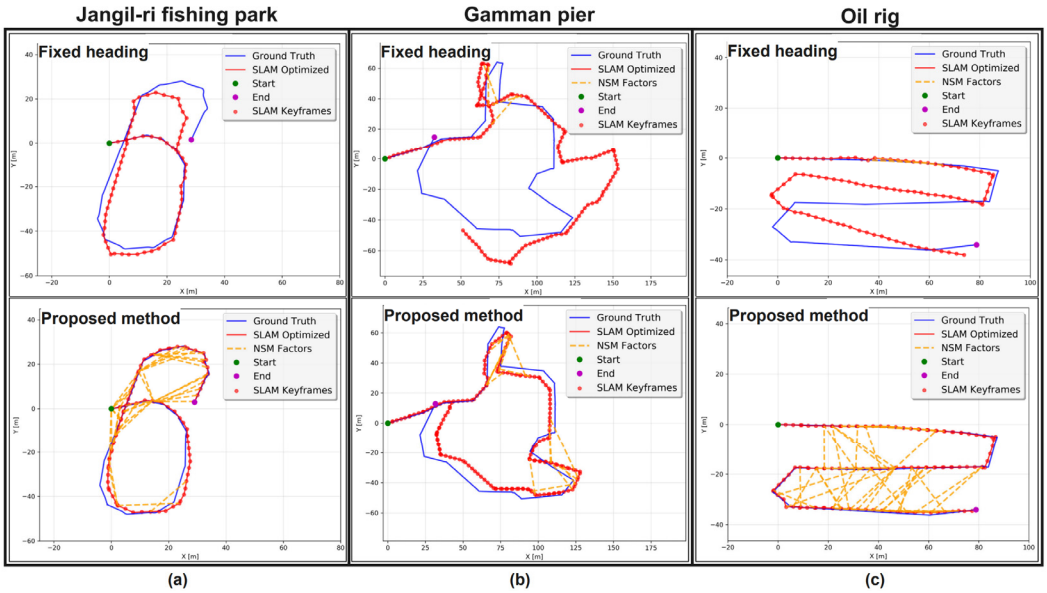

Fig. 8 Trajectory comparison results in three simulated environments using the point-to-plane ICP metric. (a) Trajectory comparison in Jangil-ri fishing park (b) Trajectory comparison in Gamman pier (c) Trajectory comparison in offshore oil rig

corresponding to $\mathbf{f}^{s}$ and $\mathbf{f}^{ns}$ respectively, were compared. In this study, convergence was not defined merely by numerical minimization of ICP, but rather by strict geometric validation. Specifically, a transformation was considered successful only if its translation $\|\Delta t\|$ and rotation $|\Delta\theta|$ were both within predefined thresholds $T_{\max}$ and $R_{\max}$, and if a sufficient number of source points retained valid nearest neighbors in the target point cloud after transformation, ensuring adequate overlap. Registrations failing to meet this overlap threshold were considered unsuccessful. Furthermore, in the NSM case, even when the above conditions were satisfied, loop closure candidates were accepted only if geometric consistency was verified through the pairwise consistency measurement (PCM) test.

6. Results

Fig. 8 visually presents the optimized SLAM trajectory comparison results between the fixed heading SLAM and the proposed method across three simulated environments relative to the ground truth. Table 1 shows that in all experimental environments, the proposed method significantly reduced RMSE of the ATE compared to the fixed-heading SLAM, even though both methods followed identical trajectories and velocities. For example, in the Jangil-ri harbor environment, the RMSE of the point-to-point ICP decreased from 4.317 m (fixed-heading SLAM) to 1.029 m with the proposed method. Similar improvements were observed across other ICP variants, such as point-to-plane and generalized-ICP(GICP), and in different environments, confirming that the proposed approach consistently enhances performance regardless of environmental conditions or ICP metric selection. Moreover, the convergence stability of ICP

registration was improved. The proposed method produced a greater number of SM and NSM factors than the fixed-heading baseline, while also exhibiting a higher ICP convergence rate. In particular, in environments dominated by planar features, factors associated with $\mathbf{K}^{o}$ provided additional geometric constraints, improving trajectory stability. Although the AUV required additional time (approximately 10 seconds on average) to stop and acquire omnidirectional features upon detecting degenerate feature sets, resulting in increased total exploration time, this trade-off was deemed acceptable. Considering the substantial improvement in localization accuracy and robustness, the proposed active viewpoint adjustment strategy effectively enhances SLAM performance in underwater environments characterized by limited geometric features.

7. Conclusions

This study addressed the issue of ICP degeneracy that frequently occurs in imaging sonar-based SLAM within planar or feature-sparse underwater structured environments. To overcome this limitation, we proposed a sonar viewpoint adjustment method that actively adjusts the viewpoint of the imaging sonar to acquire geometrically richer features. The proposed method consists of three stages: degeneracy detection, omnidirectional feature acquisition through 360° only sonar rotation, and cornerness-based next viewpoint selection. Through these steps, the system can avoid under constrained features and dynamically obtain feature sets that are favorable for reliable ICP registration. Prior to simulation experiments, a feasibility field test was conducted in a real underwater structured environment to verify the inherent scarcity of geometrically rich features in actual sonar data. The proposed method was validated in multiple simulated underwater environments, including a complex fishing park, Gamman Pier, and an offshore oil rig. Comparative experiments demonstrated that, unlike conventional SLAM systems with a fixed sonar viewpoint, the proposed method effectively mitigated ICP degeneracy and produced trajectory estimates that were more closely aligned with the ground truth, even though both methods followed identical trajectories and velocities. Furthermore, by selecting viewpoints based on cornerness, the system successfully ensured stable acquisition of feature-rich regions, thereby improving both the accuracy and robustness of SLAM.

Acknowledgments

This work was supported by the Korea Research Institute for Defense Technology Planning and Advancement (KRIT) - Grant funded by Defense Acquisition Program Administration (DAPA) (KRIT-CT-23-016, Simultaneous Localization and Mapping for UUV, 2025). And this work was also supported by the industry–academia cooperation project LIG NEX1.

References

Acosta, G.G. and Villar, S.A. (2014), “Accumulated CA–CFAR process in 2-D for online object detection from sidescan sonar data”, *IEEE J. Ocean. Eng.*, **40**(3), 558-569. https://doi.org/10.1109/JOE.2014.2320636.

Besl, P.J. and McKay, N.D. (1992), “A method for registration of 3-D shapes”, *IEEE Trans. Pattern Anal.*

Mach. Intell., **14**(2), 239-256. https://doi.org/10.1109/34.121791.
Cadena, C., Carlone, L., Carrillo, H., Latif, Y., Scaramuzza, D., Neira, J., Reid, I. and Leonard, J.J. (2016), "Past, present, and future of simultaneous localization and mapping: Toward the robust-perception age", *IEEE Trans. Robot.*, **32**(6), 1309-1332. https://doi.org/10.1109/TRO.2016.2624754.
Chen, Y. and Medioni, G. (1991), "Object modeling by registration of multiple range images", *Proceedings of the IEEE International Conference on Robotics and Automation (ICRA)*, Sacramento, CA, April. https: //doi.org/10.1109/ROBOT.1991.132043.
El-Darymli, K., McGuire, P., Power, D. and Moloney, C. (2013), "Target detection in synthetic aperture radar imagery: A state-of-the-art survey", *J. Appl. Remote Sens.*, **7**(1), 071598. https://doi.org/10.1117/1.JRS.7. 071598.
Fallon, M.F., Folkesson, J., McClelland, H. and Leonard, J.J. (2013), "Relocating underwater features autonomously using sonar-based SLAM", *IEEE J. Ocean. Eng.*, **38**(3), 500-513. https://doi.org/10.1109/JOE. 2012.2235664.
Fischler, M.A. and Bolles, R.C. (1981), "Random sample consensus: A paradigm for model fitting with applications to image analysis and automated cartography", *Commun. ACM*, **24**(6), 381-395. https://doi.org/10. 1145/358669.358692.
Fossen, T.I. (2011), *Handbook of Marine Craft Hydrodynamics and Motion Control*, John Wiley & Sons, Ltd, Chichester, UK.
Grisetti, G., Kümmerle, R., Stachniss, C. and Burgard, W. (2010), "A tutorial on graph-based SLAM", *IEEE Intell. Transp. Syst. Mag.*, **2**(4), 31-43. https://doi.org/10.1109/MITS.2010.939925.
Guth, F., Silveira, L., Botelho, S., Drews, P. and Ballester, P. (2014), "Underwater SLAM: Challenges, state of the art, algorithms and a new biologically-inspired approach", *Proceedings of the 5th IEEE RAS/EMBS International Conference on Biomedical Robotics and Biomechatronics*, São Paulo, Brazil, August. https://doi.org/10.1109/BIOROB.2014.6913908.
Harris, C. and Stephens, M. (1988), "A combined corner and edge detector", *Proceedings of the Alvey Vision Conference*, Manchester, UK, August. https://doi.org/10.5244/C.2.23.
Hatleskog, J. and Alexis, K. (2024), "Probabilistic degeneracy detection for point-to-plane error minimization", *IEEE Robot. Autom. Lett.*, **9**(12), 11234-11241. https://doi.org/10.1109/LRA.2024.3484153.
Hinduja, A., Ho, B.J. and Kaess, M. (2019), "Degeneracy-aware factors with applications to underwater SLAM", *Proceedings of the 2019 IEEE/RSJ International Conference on Intelligent Robots and Systems (IROS)*, Macau, China, November. https://doi.org/10.1109/IROS40897.2019.8968577.
Johannsson, H., Kaess, M., Englot, B., Hover, F. and Leonard, J. (2010), "Imaging sonar-aided navigation for autonomous underwater harbor surveillance", *Proceedings of the 2010 IEEE/RSJ International Conference on Intelligent Robots and Systems*, Taipei, Taiwan, October. https://doi.org/10.1109/IROS.2010.5650831.
Joshi, B., Rahman, S., Kalaitzakis, M., Cain, B., Johnson, J., Xanthidis, M., Karapetyan, N., Hernandez, A., Li, A.Q., Vitzilaios, N. and Rekleitis, I. (2019a), "Experimental comparison of open source visualinertial-based state estimation algorithms in the underwater domain", *Proceedings of the 2019 IEEE/RSJ International Conference on Intelligent Robots and Systems (IROS)*, Macau, China, November. https://doi. org/10.1109/IROS40897.2019.8968049.
Joshi, B., Xanthidis, M., Roznere, M., Burgdorfer, N.J., Mordohai, P., Li, A.Q. and Rekleitis, I. (2022), "Underwater exploration and mapping", *Proceedings of the 2022 IEEE/OES Autonomous Underwater Vehicles Symposium (AUV)*, Singapore, September. https://doi.org/10.1109/AUV53081.2022.9965805.
Lee, D., Lim, H. and Han, S. (2025), "GenZ-ICP: Generalizable and degeneracy-robust LiDAR odometry using an adaptive weighting", *IEEE Robot. Autom. Lett.*, **10**(1), 152-159. https://doi.org/10.1109/LRA. 2024.3498779.
Manhães, M.M.M., Scherer, S.A., Voss, M., Douat, L.R. and Rauschenbach, T. (2016), "UUV Simulator: A Gazebo-based package for underwater intervention and multi-robot simulation", *Proceedings of the OCEANS 2016 MTS/IEEE Monterey*, Monterey, CA, September. https://doi.org/10.1109/OCEANS.2016.7761080.

McConnell, J. and Englot, B. (2021), "Predictive 3D sonar mapping of underwater environments via objectspecific Bayesian inference", *Proceedings of the 2021 IEEE International Conference on Robotics and Automation (ICRA)*, Xi'an, China, May. https://doi.org/10.1109/ICRA48506.2021.9560737.

McConnell, J., Chen, F. and Englot, B. (2022a), "Overhead image factors for underwater sonar-based SLAM", *IEEE Robot. Autom. Lett.*, **7**(2), 4901-4908. https://doi.org/10.1109/LRA.2022.3154048.

McConnell, J., Huang, Y., Szenher, P., Collado-Gonzalez, I. and Englot, B. (2022b), "DRACo-SLAM: Distributed robust acoustic communication-efficient SLAM for imaging sonar equipped underwater robot teams", *Proceedings of the 2022 IEEE/RSJ International Conference on Intelligent Robots and Systems (IROS)*, Kyoto, Japan, October. https://doi.org/10.1109/IROS47612.2022.9981822.

McConnell, J., Collado-Gonzalez, I., Szenher, P. and Englot, B. (2025), "Large-scale dense 3-D mapping using submaps derived from orthogonal imaging sonars", *IEEE J. Ocean. Eng.*, **50**(1), 354-369. https://doi.org/10.1109/JOE.2024.3458108.

McConnell, J., Martin, J.D. and Englot, B. (2020), "Fusing concurrent orthogonal wide-aperture sonar images for dense underwater 3D reconstruction", *Proceedings of the 2020 IEEE/RSJ International Conference on Intelligent Robots and Systems (IROS)*, Las Vegas, NV, October. https://doi.org/10.1109/IROS45743.2020. 9340995.

Nakatani, T., Ura, T., Ito, Y., Kojima, J., Tamura, K., Sakamaki, T. and Nose, Y. (2008), "AUV "TUNA-SAND" and its exploration of hydrothermal vents at Kagoshima Bay", *Proceedings of the OCEANS 2008 - MTS/IEEE Kobe Techno-Ocean*, Kobe, Japan, April. https://doi.org/10.1109/OCEANSKOBE.2008.4531099.

Nashed, S.B., Jin Park, J., Webster, R. and Durham, J.W. (2021), "Robust rank deficient SLAM", *Proceedings of the 2021 IEEE/RSJ International Conference on Intelligent Robots and Systems (IROS)*, Prague, Czech Republic, September. https://doi.org/10.1109/IROS51168.2021.9636443.

Nobili, S., Tinchev, G. and Fallon, M. (2018), "Predicting alignment risk to prevent localization failure", *Proceedings of the 2018 IEEE International Conference on Robotics and Automation (ICRA)*, Brisbane, Australia, May. https://doi.org/10.1109/ICRA.2018.8462890.

Nubert, J., Walther, E., Khattak, S. and Hutter, M. (2022), "Learning-based localizability estimation for robust LiDAR localization", *Proceedings of the 2022 IEEE/RSJ International Conference on Intelligent Robots and Systems (IROS)*, Kyoto, Japan, October. https://doi.org/10.1109/IROS47612.2022.9982257.

Pan, S., Hong, Z., Hu, Z., Xu, X., Lu, W. and Hu, L. (2025), "RUSSO: Robust underwater SLAM with sonar optimization against visual degradation", *IEEE/ASME Trans. Mechatron.*, https://doi.org/10.1109/TMECH. 2025.3550730.

Pyo, J., Cho, H., Joe, H., Ura, T. and Yu, S.C. (2015), "Development of hovering type AUV "Cyclops" and its performance evaluation using image mosaicing", *Ocean Eng.*, **109**, 517-530. https://doi.org/10.1016/j.oceaneng.2015.09.023.

Rahman, S., Li, A.Q. and Rekleitis, I. (2018), "Sonar visual inertial SLAM of underwater structures", *Proceedings of the 2018 IEEE International Conference on Robotics and Automation (ICRA)*, Brisbane, Australia, May. https://doi.org/10.1109/ICRA.2018.8460545.

Rahman, S., Li, A.Q. and Rekleitis, I. (2019), "SVIn2: An underwater SLAM system using sonar, visual, inertial, and depth sensor", *Proceedings of the 2019 IEEE/RSJ International Conference on Intelligent Robots and Systems (IROS)*, Macau, China, November. https://doi.org/10.1109/IROS40897.2019.8967703.

Segal, A.V., Haehnel, D. and Thrun, S. (2009), "Generalized-ICP", *Proceedings of Robotics: Science and Systems*, Seattle, WA, June.

Singh, H., Can, A., Eustice, R., Lerner, S., McPhee, N. and Roman, C. (2004), "Seabed AUV offers new platform for high-resolution imaging", *Eos Trans. Am. Geophys. Union*, **85**(31), 289-296. https://doi.org/10.1029/2004EO310002.

Song, J., Bagoren, O., Andigani, R., Sethuraman, A. and Skinner, K.A. (2024), "TURTLMap: Real-time localization and dense mapping of low-texture underwater environments with a low-cost unmanned underwater vehicle", *Proceedings of the 2024 IEEE/RSJ International Conference on Intelligent Robots and Systems (IROS)*, Abu Dhabi, UAE, October. https://doi.org/10.1109/IROS58592.2024.10801692.

Stokey, R.P., Roup, A., von Alt, C., Allen, B., Forrester, N., Austin, T., Goldsborough, R., Purcell, M., Jaffre, F., Packard, G. and Kukulya, A. (2005), "Development of the REMUS 600 autonomous underwater vehicle", *Proceedings of the OCEANS 2005 MTS/IEEE*, Washington, DC, September. https://doi.org/10.1109/ OCEANS.2005.1639934.

Sun, K., Cui, W. and Chen, C. (2021), "Review of underwater sensing technologies and applications", *Sensors*, **21**(23), 7849. https://doi.org/10.3390/s21237849.

Tuna, T., Nubert, J., Nava, Y., Khattak, S. and Hutter, M. (2024), "X-ICP: Localizability-aware LiDAR registration for robust localization in extreme environments", *IEEE T. Robot.*, **40**, 452-471. https: //doi.org/10.1109/TRO.2023.3335691.

Wang, J., Chen, F., Huang, Y., McConnell, J., Shan, T. and Englot, B. (2022), "Virtual maps for autonomous exploration of cluttered underwater environments", *IEEE J. Ocean. Eng.*, **47**(4), 916-935. https://doi.org/ 10.1109/JOE.2022.3153897.

Westman, E., Hinduja, A. and Kaess, M. (2018), "Feature-based SLAM for imaging sonar with underconstrained landmarks", *Proceedings of the 2018 IEEE International Conference on Robotics and Automation (ICRA)*, Brisbane, Australia, May. https://doi.org/10.1109/ICRA.2018.8461004.

Wu, T.P., Yeung, S.K., Jia, J., Tang, C.K. and Medioni, G. (2012), "A closed-form solution to tensor voting: Theory and applications", *IEEE T. Pattern Anal.*, **34**(8), 1482-1495. https://doi.org/10.1109/TPAMI.2011.250.

Xu, S., Zhang, K. and Wang, S. (2025), "AQUA-SLAM: Tightly coupled underwater acoustic-visual-inertial SLAM with sensor calibration", *IEEE T. Robot.*, **41**, 2785-2803. https://doi.org/10.1109/TRO.2025.3554396.

Zhang, J., Kaess, M. and Singh, S. (2016), "On degeneracy of optimization-based state estimation problems", *Proceedings of the 2016 IEEE International Conference on Robotics and Automation (ICRA)*, Stockholm, Sweden, May. https://doi.org/10.1109/ICRA.2016.7487211.

Zhang, M.M., Choi, W.S., Herman, J., Davis, D., Vogt, C., McCarrin, M., Vijay, Y., Dutia, D., Lew, W., Peters, S. and Bingham, B. (2022), "DAVE aquatic virtual environment: Toward a general underwater robotics simulator", *Proceedings of the 2022 IEEE/OES Autonomous Underwater Vehicles Symposium (AUV)*, Singapore, September. https://doi.org/10.1109/AUV53081.2022.9965808.

Zhao, L., Zhou, M. and Loose, B. (2023), "Tightly-coupled visual-DVL-inertial odometry for robot-based icewater boundary exploration", *Proceedings of the 2023 IEEE/RSJ International Conference on Intelligent Robots and Systems (IROS)*, Detroit, MI, October. https://doi.org/10.1109/IROS55552.2023.10342024.

MK